Device Architectures for Enhanced Photon Recycling in Thin-Film Multijunction Solar Cells

*Xing Sheng, Myoung Hee Yun, Chen Zhang, Ala'a M. Al-Okaily, Maria Masouraki, Ling Shen, Shuodao Wang, William L. Wilson, Jin Young Kim, Placid Ferreira, Xiuling Li, Eli Yablonovitch, and John A. Rogers**

Multijunction (MJ) solar cells have the potential to operate across the entire solar spectrum, for ultrahigh efficiencies in light to electricity conversion. Here an MJ cell architecture is presented that offers enhanced capabilities in photon recycling and photon extraction, compared to those of conventional devices. Ideally, each layer of a MJ cell should recycle and re-emit its own luminescence to achieve the maximum possible voltage. This design involves materials with low refractive indices as interfaces between sub-cells in the MJ structure. Experiments demonstrate that thin-film GaAs devices printed on low-index substrates exhibit improved photon recycling, leading to increased open-circuit voltages (V_{oc}), consistent with theoretical predictions. Additional systematic studies reveal important considerations in the thermal behavior of these structures under highly concentrated illumination. Particularly when combined with other optical elements such as anti-reflective coatings, these architectures represent important aspects of design for solar cells that approach thermodynamic efficiency limits for full spectrum operation.

1. Introduction

In the past few decades, significant research has sought to realize thermodynamic efficiency limits in different types of photovoltaic (PV) cells.[1–4] Such efforts are motivated by the substantial reductions in the cost of energy with improved PV system efficiencies.[5] Single junction cells made using semiconductors such as gallium arsenide (GaAs) have a theoretical limit in efficiency of about 33.4% under one sun illumination, primarily due to the ineffective use of the entire solar spectrum.[1] Multijuction (MJ) cells, by contrast, spectrally split sunlight into sub-cells with different bandgaps, thereby providing pathways to greatly improved efficiencies.[6–13] Conventional MJ cells require lattice matched or metamorphic epitaxial growth of the individual sub-cells. In addition, the serially connected sub-cells are constrained by current matching since the photocurrent of a two-terminal MJ device is determined by the smallest current among the sub-cells. These considerations constrain options in material selection, thereby creating practical challenges to the growth of more than three junctions in high performance cells. Our recent work demonstrates the ability to use printing techniques to assemble microscale, multijunction, multi-terminal cells with refractive-index matched interfaces, to yield ultrahigh cell and module efficiencies.[13]

In spite of the promise of such approaches, interfaces that are index matched are unable to recycle and extract infrared photons needed to approach the detailed balance efficiency limit.[14] **Figure 1**a illustrates the challenge in a simple example of a stack of two sub-cells with a refractive-index matched (high-index) interface, to minimize interface reflection losses. The high bandgap top cell absorbs photons with energies above its bandgap ($h\nu_1 > h\nu_g$, where $h\nu_g$ is the bandgap of the top cell),

Dr. X. Sheng, Dr. S. Wang, Dr. W. L. Wilson, Prof. J. A. Rogers
Department of Materials Science and Engineering
and Frederick Seitz Materials Research Laboratory
University of Illinois at Urbana-Champaign
Urbana, IL 61801, USA
E-mail: jrogers@illinois.edu

M. H. Yun, Prof. J. Y. Kim
School of Energy and Chemical Engineering
Ulsan National Institute of Science and Technology (UNIST)
Ulsan 689–798, Republic of Korea

C. Zhang, Prof. X. Li
Department of Electrical and Computer Engineering
University of Illinois at Urbana-Champaign
Urbana, IL 61801, USA

A. M. Al-Okaily, Prof. P. Ferreira
Department of Mechanical Science and Engineering
University of Illinois at Urbana-Champaign
Urbana, IL 61801, USA

M. Masouraki
Department of Physics
University of Illinois at Urbana-Champaign
Urbana, IL 61801, USA

Dr. L. Shen
Department of Physics, College of Sciences
China University of Mining and Technology
Xuzhou, Jiangsu 221116, P. R. China

Prof. E. Yablonovitch
Department of Electrical Engineering and Computer Sciences
University of California, Berkeley
Berkeley, CA 94720, USA

DOI: 10.1002/aenm.201400919

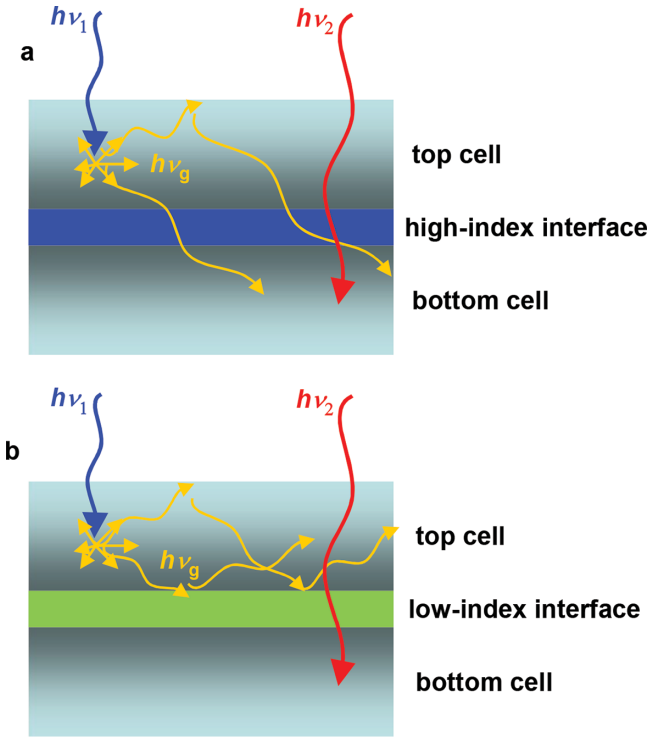

Figure 1. Schematic illustrations of photon dynamics in MJ solar cells with a) a high-index interface and b) a low-index interface.

while the low bandgap bottom cell absorbs low energy photons below the bandgap of the top cell ($h\nu_2 < h\nu_g$). When the top cell operates at the open-circuit voltage (V_{oc}), photo-generated electron-hole pairs recombine. As described subsequently, most (≈99%) of the isotropically emitted photons ($h\nu_g$) generated by radiative recombination are trapped in the stacked device and absorbed by the bottom cell. As a result, the decreased external luminescent efficiency due to inefficient photon recycling leads to a reduced V_{oc} for the top cell.[14]

Here, we propose an MJ cell design that minimizes this limitation, through the use of a low-index interface material. As shown in Figure 1b, photons from the top cell ($h\nu_g$) that emit outside the escape cone (at angles greater than the critical angle) undergo total internal reflection, without entering the bottom cell where they would be absorbed. The angle averaged reflectance at the low-index interface can be estimated by

$$\bar{R} = \int_0^{\frac{\pi}{2}} R(\theta)\sin\theta\,d\theta = \int_0^{\theta_c} R(\theta)\sin\theta\,d\theta + \cos\theta_c \quad (1)$$

where θ_c is the critical angle for total internal reflection at the interface ($\sin\theta_c = n_{interface}/n_{cell}$), $n_{interface}$ and n_{cell} are the refractive indices of the interface material and the solar cell material, respectively, and $R(\theta)$ is reflectance at the interface for light with different propagation angles and polarizations, which can be calculated by the transfer-matrix method. This expression indicates that $\bar{R}$ increases with the difference between the index of the cell and the interface material. For the case of a GaAs top cell (n_{cell} = 3.5) and an air gap interface ($n_{interface}$ = 1.0), $\bar{R}$ is ≈98%. A high degree of photon recycling can be enabled in this way. The outcome is an increased external luminescent efficiency and V_{oc} for the top cell.[15] At the same time, normally incident low energy photons ($h\nu_2 < h\nu_g$) can pass through the interface to reach the bottom cell. Anti-reflective coatings (ARCs) can be used to minimize reflection losses for low energy photons without affecting $\bar{R}$ for isotropically re-emitted photons, as described subsequently.

2. Results and Discussion

The luminescent properties of thin-film semiconductor layers on substrates with different refractive indices reveal essential aspects of the photon recycling processes, as shown in **Figure 2**. Here, GaAs-based double heterostructure (DH) thin films (100 nm $Al_{0.3}Ga_{0.7}As$/1000 nm GaAs/100 nm $Al_{0.3}Ga_{0.7}As$) act as active device layers. The DHs are grown on a GaAs wafer with a lattice matched $Al_{0.95}Ga_{0.05}As$ sacrificial layer, to enable release by epitaxial liftoff. Figure 2a schematically illustrate these layers on a GaAs substrate (unreleased), and transfer printed onto a glass substrate with a 25 μm thick layer of a photo-definable epoxy (SU-8) layer, and onto a glass substrate with a 25 μm thick air gap in between. The SU-8 layer and the air gap are sufficiently thick that the underlying glass substrates have negligible effects on the evanescent photon outcoupling from the GaAs DH layers. Figure 2b presents photoluminescence (PL) decay measurements for these various substrates (GaAs, SU-8 and air) under excitation at 776 nm. At high carrier densities, the radiative recombination lifetimes, τ, are (0.46 ± 0.03) ns, (1.64 ± 0.01) ns and (2.22 ± 0.14) ns, for GaAs DH layers on GaAs, SU-8 and air, respectively. These results are consistent with inhibition of spontaneous emission by use of low-index substrates and, therefore, significant enhancements in the emission lifetime as well as the photon recycling.[16,17] Figure 2c plots $1/\tau$ as a function of n_{sub}^2+1, where n_{sub} is the refractive index of the substrate material (n_{sub} = 3.5, 1.5 and 1.0 for GaAs, SU-8 and air, respectively). The linear relationship between $1/\tau$ and n_{sub}^2+1 is consistent with theory.[16]

Figure 3a shows microscale, thin-film GaAs solar cells placed on different substrates using similar epitaxial liftoff and printing approaches. The cells (with an active device area of about 0.39 mm^2) use a vertical GaAs homojunction with metallized contacts on both p and n sides (Figure 3b,c). Figure 3d presents a representative cell on a patterned film of SU-8, where the majority of the cell area remains suspended over an air gap (25 μm thick). Figure 3e plots the corresponding current-voltage response under one-sun illumination (AM1.5g spectrum). The cell (without an ARC) reaches a short-circuit current (I_{sc}) of 62.8 μA, an V_{oc} of 0.96 V and a fill factor (FF) of 82%, corresponding to an efficiency of ≈12.7%.

As demonstrated in Figure 2b, the refractive index of the substrate medium affects the spontaneous emission rate and the photon recycling processes. Analytically, the V_{oc} can be expressed as[18]

$$V_{oc} = V_{db} + \frac{kT}{q}\ln(\eta_{ext}) = V_{db} + \frac{kT}{q}\ln\left(\frac{\eta_{int}\overline{P_{esc}}}{1-\eta_{int}\overline{P_{abs}}}\right) \quad (2)$$

where V_{db} is the ideal V_{oc} obtained at the detailed balance limit, η_{ext} is the external luminescent efficiency for the emitted photons escaping from the cell front surface, η_{int} is the internal luminescent efficiency, and $\overline{P_{esc}}$ and $\overline{P_{abs}}$ are

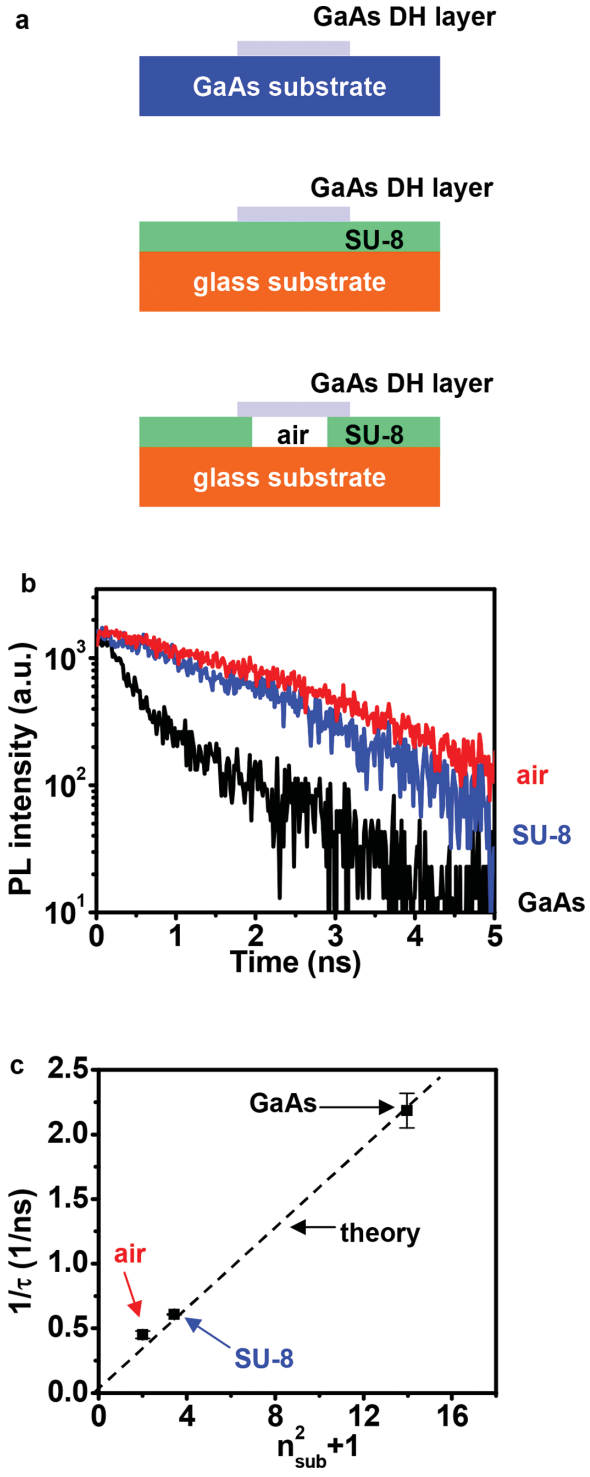

Figure 2. a) Schematic illustrations of GaAs DH layers on substrates with different interface materials. b) Measured PL intensity decays. c) Plot of the relationship between PL decay lifetime τ and interface refractive index n. In agreement with theory, $1/\tau$ is linearly proportional to n_{sub}^2+1.

the averaged probabilities of photon escape and re-absorption, respectively. $\overline{P_{esc}}$ and $\overline{P_{abs}}$ are determined by the optical properties of the GaAs device layers as well as the substrate index n.

Figure 4a shows the relationship between V_{oc} and substrate index n, for different η_{int}. Since increases in n lead to reductions in $\overline{P_{esc}}$ and increases in $\overline{P_{abs}}$, V_{oc} decreases monotonically with n. These analytical results are qualitatively consistent with one-sun current-voltage measurements (Figure 4b and 4c) on multiple GaAs cells (≈30 cells) placed on different substrates, as shown in Figure 3a. The cells printed on Si substrates with low-index interfaces (air gap and SU-8) exhibit higher V_{oc} (0.970 V ± 0.003 V and 0.973 V ± 0.003 V for air and SU-8 interfaces, respectively) than unreleased cells on high-index GaAs substrates (0.959 V ± 0.003 V). The I_{sc} for all the cells remain similar. The averaged one-sun efficiencies are increased from 12.7% for unreleased GaAs cells to about 12.8% for cells with air and SU-8 interfaces. The experimental values of V_{oc} (0.95–0.98 V) are lower than the theoretically calculated values (1.05–1.15 V), likely due to the non-optimal electrical design, which leads to a lower V_{db}. The averaged V_{oc} measured for the cells with the air gap interface are lower than that for cells with the SU-8 interface. This deviation from theoretical predictions is likely associated with the mechanical instabilities (for example, slight bowing) for the cells suspended over the air gaps, as well as measurement variations. As discussed below, one-sun illumination induces negligible temperature changes for all the cells on various substrates. Therefore, thermal effects can be excluded as a source of variations in V_{oc} and I_{sc}.

The most practical embodiments MJ cells for terrestrial use require optical concentrators, to enable low-cost and high-efficiency operation. Under high power irradiance, thermal management is critically important. A focused laser beam (488 nm, tunable power) incident on cells with different substrates shown in Figure 3a serves to simulate the thermal effects of concentrated sunlight. **Figure 5**a compares the experiential and the simulated (using steady state conjugate heat transfer finite element model) maximum temperatures on the surfaces of the cells, as a function of absorbed laser power between 0 and 0.13 W. Under irradiance power equivalent to one-sun illumination (≈5×10^{-4} W), temperature changes are negligible for all cases. As the power increases, temperatures increase for cells with air gap and SU-8 interfaces, while the temperatures for cells on GaAs remain close to room temperature. Figure 5b presents measured and simulated temperature distributions (map size: 0.7 mm × 0.7 mm) on the cell surfaces for an absorbed laser power of 0.13 W, which is equivalent to the irradiance power at a concentration level of about 250 suns. The maximum surface temperatures for air gap, SU-8 and GaAs interfaces are measured to be 134 °C, 56 °C and 22 °C, respectively, which agree with the simulation results. These temperature differences can be attributed to differences in thermal conductivities of the different interface materials (0.02 W/m/K for air, 0.2 W/m/K for SU-8 and 55 W/m/K for GaAs). The results suggest that thermal management is important to consider, particularly for low-index interfaces that have low thermal conductivity (e.g., air gap or SU-8). An effective way to minimize increases in cell temperature is to reduce the thickness of the low index material, as shown for the case of an air gap in Figure 5c. Here, the calculated maximum temperature decreases from 130 °C to 20 °C, as the gap size decreases from 25 μm to 0 μm. Meanwhile, the optical reflectance at the interface (calculated using Equation (1) decreases as the gap size approaches the

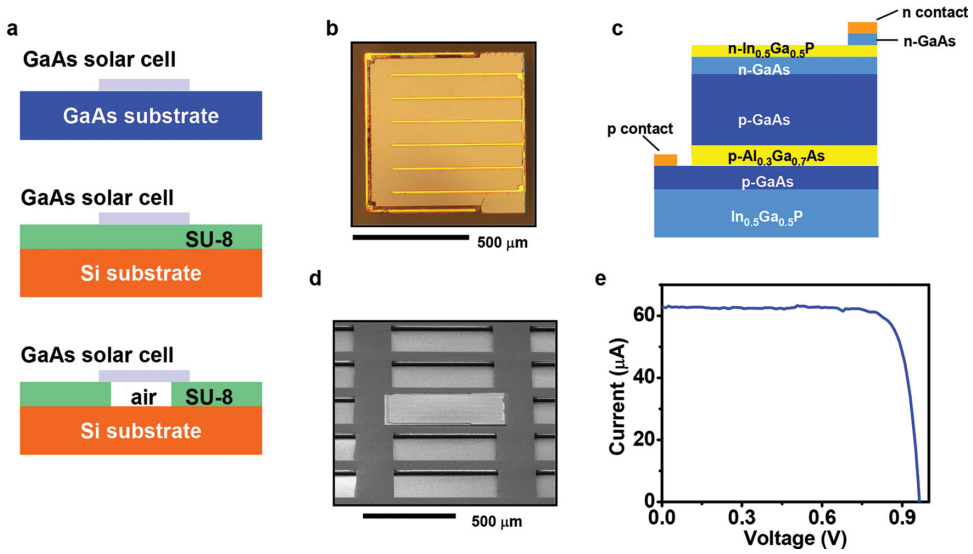

Figure 3. a) Schematic illustrations of GaAs microscale solar cells on substrates with different interface materials. b) Optical microscopy image (top view) of a GaAs cell (0.7 mm × 0.7 mm) with ohmic contacts. c) Cross sectional device layout of the GaAs cell. d) SEM image (tilted view) of a GaAs cell printed on patterned SU-8, with a 25 μm air gap in between. e) Measured current-voltage characteristic for a GaAs cell under AM1.5g illumination.

sub-wavelength scale, due to the increased evanescent coupling. Air gaps of ≈200–1000 nm balance these competing considerations in optical and thermal performance. The inset of Figure 5c illustrates the measured temperature distribution for a GaAs cell printed on a Si substrate with a 500 nm thick air gap interface. The maximum cell temperature is around 35 °C, in agreement with the numerical calculation.

The results demonstrated here indicate that MJ device architectures with low-index interfaces can effectively improve V_{oc} for the top cell due to enhanced photon recycling processes. To enable low energy photons to pass through the top cell and reach the bottom cell with minimized losses, anti-reflective coatings can be introduced between the cells and the low-index interface materials (air or SU-8), as illustrated in **Figure 6**a. While these ARCs allow low energy photons to pass through the top cell, total internal reflection (TIR) conditions remain for re-emitted photons, since the critical angle θ_c for TIR is still determined by the solar cell material and the low-index interface material ($\sin\theta_c = n_{air}/n_{cell}$). As a result, photon recycling processes inside the top cell are largely unaffected by the ARCs.

Figure 6b shows a proof-of-concept device layout made using a silicon/germanium (Si/Ge) stacked structure with an air gap interface. More realistic device demonstrations can be achieved using semiconductors with high luminescence efficiencies such as GaAs and InGaAs. A thin-film Si layer (size 0.7 mm × 0.7 mm, thickness 10 μm) released from a silicon-on-insulator wafer printed onto a Ge substrate with patterned posts of SU-8 forms a 25 μm thick air gap in between. A 150 nm thick layer of HfO_2 ($n \approx 2.0$) formed on both front and back surfaces of the Si as well as the front surface of the Ge, using atomic layer deposition (ALD), forms an ARC. Reflection spectra measured and simulated for the Si/air gap/Ge stacked structures with and without ARCs appear in Figure 6c,d, respectively, for wavelengths between 1150 nm and 1800 nm, where photons can pass through the Si to be absorbed by the Ge. The introduction of ARCs greatly suppresses the Fresnel reflection losses at the cell/air interfaces, by reducing the averaged reflectance from 61% (without ARCs) to 13% (with ARCs). Further improvements in optical efficiencies can be achieved, for example, by using multilayered ARCs at all of the cell surfaces.[19]

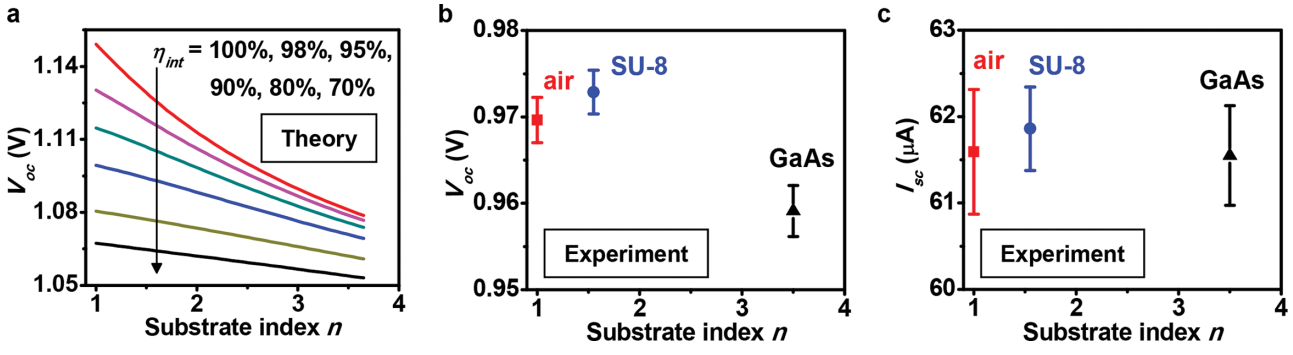

Figure 4. a) Calculated behavior of V_{oc} for ideal GaAs cells on substrates with different refractive indices, at different internal luminescent efficiency η_{int}. b) Measured V_{oc} for micro GaAs cells on different substrates (air, SU-8 and GaAs). c) Measured I_{sc} for micro GaAs cells on different substrates (air, SU-8 and GaAs).

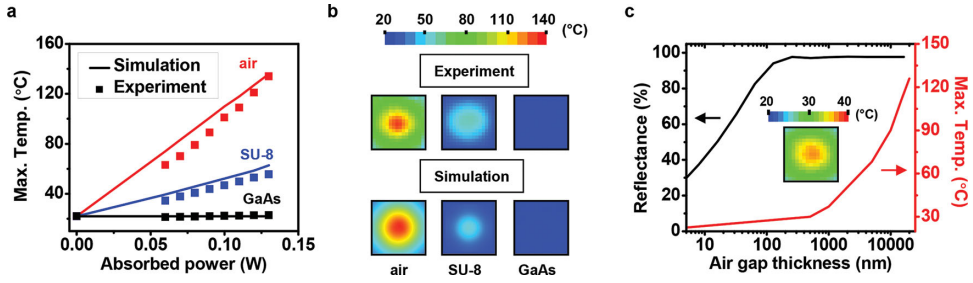

Figure 5. a) Simulated and measured maximum temperatures reached on the front surfaces for cells on different substrates, as a function of absorbed laser power. b) Measured and simulated temperature distributions on cell surfaces with an absorbed laser power of 0.13 W. Map size: 0.7 mm × 0.7 mm. c) Simulated optical reflectance at the cell/air gap interface and maximum temperature for a cell with the air gap interface with an absorbed laser power of 0.13 W, as a function of the air gap thickness. Inset: measured temperature distributions on a GaAs cell printed on Si with a 500 nm thick air gap.

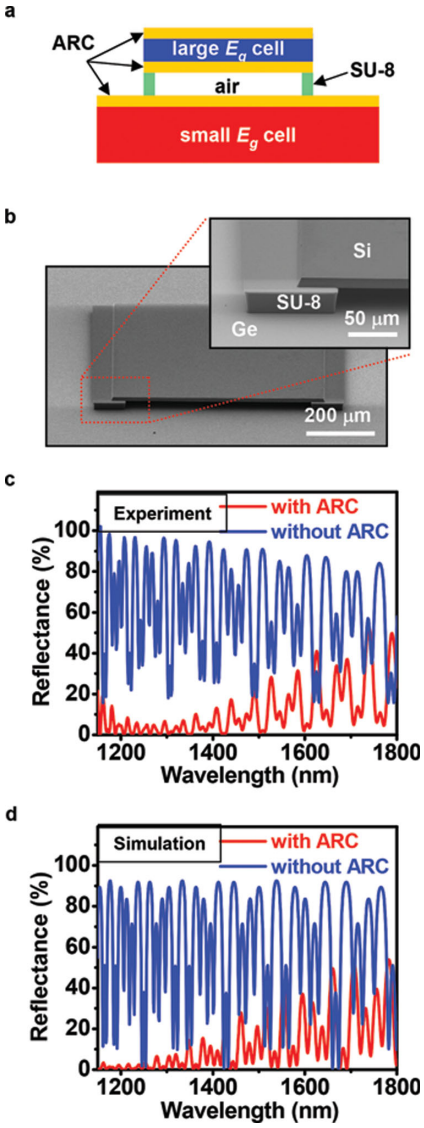

Figure 6. a) Schematic illustration of a MJ cell structure with an air gap interface and ARCs at all the semiconductor/air interfaces. b) SEM image (tilted view) of a Si thin film (size 0.7 mm × 0.7 mm, 10 μm thick) printed on a Ge substrate with an air gap interface formed by patterned SU-8 posts, as a proof of concept demonstration. c) Measured and d) simulated reflectance spectra for the Si/air gap/Ge stacked structures with and without ARCs made by 150 nm ALD HfO_2.

3. Conclusion

In summary, the results presented here illustrate an MJ solar cell architecture in which efficiency improvements are achieved by using low refractive index interfaces between different subcells. Released thin-film GaAs micro cells printed on structures with low-index air and SU-8 interfaces exhibit enhanced photon recycling effects and thus increased V_{oc}. This device design can be applied to practical MJ devices, such as InGaP/GaAs double junction or InGaP/GaAs/InGaAs triple junction cells, with potential to reach higher cell efficiencies than those possible with conventional devices and to eliminate requirements of lattice and current matching. In addition, vertically stacked device architectures realized by processes of epitaxial liftoff and transfer printing avoid complexities in optical design associated with other spectral splitting methods.[20,21] For cells that operate under high concentrations, additional issues in thermal management must be considered. Thermally conductive interface materials such as low-index oxides or fluids might be used to replace air or SU-8, thereby facilitating heat dissipation. The collective set of design and assembly concepts presented here provide potential routes to PV devices that further approach thermodynamic limits in efficiency.

4. Experimental Section

Fabrication of GaAs Double Heterostructures (DH) and Micro Solar Cells: The GaAs DH and solar cell device structures were grown on GaAs substrates using metal-organic chemical vapor deposition (MOCVD). The DH structure (from bottom to top) included: the GaAs substrate, a 500 nm $Al_{0.95}Ga_{0.05}As$ sacrificial layer, a 5 nm GaAs protection layer, a 100 nm n-$Al_{0.3}Ga_{0.7}As$ ($n = 3 \times 10^{18}$ cm^{-3}), a 1000 nm p-GaAs ($p = 5 \times 10^{17}$ cm^{-3}), a 100 nm p-$Al_{0.3}Ga_{0.7}As$ ($p = 3 \times 10^{18}$ cm^{-3}), and another 5 nm GaAs protection layer. The solar cell structure (from bottom to top) included: the GaAs substrate, a 500 nm $Al_{0.95}Ga_{0.05}As$ sacrificial layer, a 700 nm $In_{0.5}Ga_{0.5}P$ supporting layer, a 300 nm p-GaAs ($p = 3 \times 10^{19}$ cm^{-3}) bottom contact layer, a 100 nm p-$Al_{0.3}Ga_{0.7}As$ ($p = 5 \times 10^{18}$ cm^{-3}) back surface field (BSF) layer, a 2500 nm p-GaAs ($p = 1 \times 10^{17}$ cm^{-3}) base layer, a 100 nm n-GaAs ($n = 2 \times 10^{18}$ cm^{-3}) emitter layer, a 25 nm n-$In_{0.5}Ga_{0.5}P$ ($n = 2 \times 10^{18}$ cm^{-3}) window layer and a 200 nm n-GaAs ($n = 1 \times 10^{19}$ cm^{-3}) top contact layer. Zn and Si served as p-type and n-type dopants, respectively. 10 nm Cr/200 nm Au served as electrical contacts. The DH and solar cell devices (size 0.7 mm × 0.7 mm) were lithographically fabricated, with the $Al_{0.95}Ga_{0.05}As$ sacrificial layer removed by a hydrofluoric acid (HF) based solution (ethanol:HF = 1.5:1 by volume).[22,23] Subsequently, individual DH and solar cells devices were transfer printed onto other substrates (glass and Si) with different interfaces (air gap and SU-8) using shaped

PDMS stamps.[24] The air gaps (0.5 mm × 0.5 mm) were formed by lithographically defined patterns in SU-8 (25 μm thick).

Device Characterization: Photoluminescence (PL) decay measurements were performed using GaAs DH layers printed on different substrates. Excitation light was generated by using a supercontinuum laser (NKT Photonics EXR-15) passed through a bandpass filter (center wavelength 776 nm, FWHM = 10 nm). PL intensity was collected by a single photon detector (ID Quantique id100–20). The current-voltage curves of GaAs solar cells were measured by a Keithley 2400 source meter under standard AM1.5g illumination.

Thermal Measurement and Modeling: Steady-state temperature distributions on the top surface of microcells on different substrates were measured by a thermal imaging camera (FLIR A655sc), under irradiance generated with an argon laser beam (center wavelength 488 nm, Gaussian beam width 0.35 mm, TM polarized). A 3D steady-state heat transfer finite element analysis model was developed (COMSOL Multiphysics) to evaluate the temperature rise during the laser heating. The model accounted for the heat transfer through different interfaces (air, SU-8 and GaAs) underneath the cells, as well as the natural heat convection to the atmosphere due to air interaction with cell surfaces. Furthermore, the thermal radiation from cells to the atmosphere was included in the model assuming an emissivity of 0.7 for GaAs. It should be noted that near-field heat transfer effects were not taken into account into our model, which may cause some deviations at sub-micrometer length scales.

Optical Reflection Measurement and Modeling: Infrared reflectance spectra for the Si/air gap/Ge stacked structures with and without ARCs were measured using a microscope-coupled Fourier transform infrared (FTIR) spectrometer (Bruker Vertex). The transfer matrix method was used to simulate optical reflections of the multilayer structures.

Acknowledgements

This work was supported by the DOE "Light-Material Interactions in Energy Conversion" Energy Frontier Research Center under grant DE-SC0001293. L.S. acknowledges support from the China Scholarship Council.

Received: June 3, 2014
Revised: July 9, 2014
Published online:

[1] W. Shockley, H. J. Queisser, *J. Appl. Phys.* **1961**, *32*, 510.
[2] A. Polman, H. A. Atwater, *Nat. Mater.* **2012**, *11*, 174.
[3] A. Luque, *J. Appl. Phys.* **2011**, *110*, 031301.
[4] M. A. Green, K. Emery, Y. Hishikawa, W. Warta, E. D. Dunlop, *Prog. Photovolt: Res. Appl.* **2014**, *22*, 1.
[5] C. Breyer, A. Gerlach, *Prog. Photovolt: Res. Appl.* **2013**, *21*, 121.
[6] K. A. Bertness, S. R. Kurtz, D. J. Friedman, A. E. Kibbler, C. Kramer, J. M. Olson, *Appl. Phys. Lett.* **1994**, *65*, 989.
[7] D. Derkacs, R. Jones-Albertus, F. Suarez, O. Fidaner, *J. Photonics Energy* **2012**, *2*, 021805.
[8] R. R. King, D. C. Law, K. M. Edmondson, C. M. Fetzer, G. S. Kinsey, H. Yoon, R. A. Sherif, N. H. Karam, *Appl. Phys. Lett.* **2007**, *90*, 183516.
[9] J. F. Geisz, S. Kurtz, M. W. Wanlass, J. S. Ward, A. Duda, D. J. Friedman, J. M. Olson, W. E. McMahon, T. E. Moriarty, J. T. Kiehl, *Appl. Phys. Lett.* **2007**, *91*, 023502.
[10] R. R. King, A. Boca, W. Hong, X. Q. Liu, D. Bhusari, D. Larrabee, K. M. Edmondson, D. C. Law, C. M. Fetzer, S. Mesropian, N. H. Karam, *Proc. 24th Euro. Photovolt. Solar Energy Conf.* **2009**, 55.
[11] S. Wojtczuk, P. Chiu, X. Zhang, D. Pulver, C. Harris, B. Siskavich, *AIP Conf. Proc.* **2011**, *1407*, 9.
[12] K. Sasaki, T. Agui, K. Nakaido, N. Takahashi, R. Onitsuka, T. Takamoto, *AIP Conf. Proc.* **2013**, *1556*, 22.
[13] X. Sheng, C. A. Bower, S. Bonafede, J. W. Wilson, B. Fisher, M. Meitl, H. Yuen, S. Wang, L. Shen, A. R. Banks, C. J. Corcoran, R. G. Nuzzo, S. Burroughs, J. A. Rogers, *Nat. Mater.* **2014**, *13*, 593.
[14] O. D. Miller, E. Yablonovitch, S. R. Kurtz, *IEEE J. Photovolt.* **2012**, *2*, 303.
[15] V. Ganapati, C. S. Ho, E. Yablonovitch, arXiv:1406.3126, http://arxiv.org/abs/1406.3126.
[16] E. Yablonovitch, T. J. Gmitter, R. Bhat, *Phys. Rev. Lett.* **1988**, *61*, 2546.
[17] P. Renaud, F. Raymond, B. Bensaid, C. Verie, *J. Appl. Phys.* **1992**, *71*, 1907.
[18] M. A. Steiner, J. F. Geisz, I. Garcia, D. J. Friedman, A. Duda, S. R. Kurtz, *J. Appl. Phys.* **2013**, *113*, 123109.
[19] L. Zhao, G. Flamand, J. Poortmans, *AIP Conf. Proc.* **2010**, *1277*, 284.
[20] A. Barnett, D. Kirkpatrick, C. Honsberg, D. Moore, M. Wanlass, K. Emery, R. Schwartz, D. Carlson, S. Bowden, D. Aiken, A. Gray, S. Kurtz, L. Kazmerski, M. Steiner, J. Gray, T. Davenport, R. Buelow, L. Takacs, N. Shatz, J. Bortz, O. Jani, K. Goossen, F. Kiamilev, A. Doolittle, I. Ferguson, B. Unger, G. Schmidt, E. Christensen, D. Salzman, *Prog. Photovolt: Res. Appl.* **2009**, *17*, 75.
[21] J. D. McCambridge, M. A. Steiner, B. L. Unger, K. A. Emery, E. L. Christensen, M. W. Wanlass, A. L. Gray, L. Takacs, R. Buelow, T. A. McCollum, J. W. Ashmead, G. R. Schmidt, A. W. Haas, J. R. Wilcox, J. Van Meter, J. L. Gray, D. T. Moore, A. M. Barnett, R. J. Schwartz, *Prog. Photovolt: Res. Appl.* **2011**, *19*, 352.
[22] X. Sheng, L. Shen, T. Kim, L. Li, X. Wang, R. Dowdy, P. Froeter, K. Shigeta, X. Li, R. G. Nuzzo, N. C Giebink, J. A. Rogers, *Adv. Energy Mater.* **2013**, *3*, 991.
[23] X. Sheng, C. J. Corcoran, J. He, L. Shen, S. Kim, J. Park, R. G. Nuzzo, J. A. Rogers, *Phys. Chem. Chem. Phys.* **2013**, *15*, 20434.
[24] A. Carlson, H. J. Kim-Lee, J. Wu, P. Elvikis, H. Cheng, A. Kovalsky, S. Elgan, Q. Yu, P. M. Ferreira, Y. Huang, K. T. Turner, J. A. Rogers, *Appl. Phys. Lett.* **2011**, *98*, 264104.